


RESEARCH ARTICLE

Summertime cloud phase strongly influences surface melting on the Larsen C ice shelf, Antarctica

E. Gilbert^{1,2}  | A. Orr¹ | J. C. King¹ | I. A. Renfrew²  | T. Lachlan-Cope¹ | P. F. Field^{3,4} | I. A. Boutle³

¹British Antarctic Survey, Cambridge, UK

²School of Environmental Sciences,
University of East Anglia, Norwich, UK

³Met Office, Exeter, UK

⁴University of Leeds, Leeds, UK

Correspondence

E. Gilbert. British Antarctic Survey,
Madingley Road, Cambridge CB3 0ET, UK
Email: ellgil82@bas.ac.uk

Funding information

Natural Environment Research Council,
Grant/Award Number: NE/L002582

Abstract

Surface melting on Antarctic Peninsula ice shelves can influence ice shelf mass balance, and consequently sea level rise. We show that summertime cloud phase on the Larsen C ice shelf on the Antarctic Peninsula strongly influences the amount of radiation received at the surface and can determine whether or not melting occurs. While previous work has separately evaluated cloud phase and the surface energy balance (SEB) during summertime over Larsen C, no previous studies have examined this relationship quantitatively. Furthermore, regional climate models frequently produce surface radiation biases related to cloud ice and liquid water content. This study uses a high-resolution regional configuration of the UK Met Office Unified Model (MetUM) to assess the influence of cloud ice and liquid properties on the SEB, and consequently melting, over the Larsen C ice shelf. Results from a case-study show that simulations producing a vertical cloud phase structure more comparable to aircraft observations exhibit smaller surface radiative biases. A configuration of the MetUM adapted to improve the simulation of cloud phase reproduces the observed surface melt most closely. During a five-week simulation of summertime conditions, model melt biases are reduced to $<2 \text{ W}\cdot\text{m}^{-2}$: a four-fold improvement on a previous study that used default MetUM settings. This demonstrates the importance of cloud phase in determining summertime melt rates on Larsen C.

KEYWORDS

Antarctic Peninsula, cloud phase, Larsen C ice shelf, regional climate modelling, surface energy balance, surface melt

1 | INTRODUCTION

Despite their importance in the polar climate system, Antarctic clouds are among the most under-sampled in the world because of the difficulties of *in situ* data collection in this harsh, remote environment (Lachlan-Cope, 2010; Bromwich *et al.*, 2012). The effect of Antarctic clouds on the amount of energy at the surface (the surface energy balance, SEB) can determine whether the ice surface remains frozen or melts (Kalesse *et al.*, 2016; Nicolas *et al.*, 2017), with consequent implications for ice sheet mass balance and, potentially, for global sea level rise. Cloud impacts on SEB are most important in warmer regions like the Antarctic Peninsula, where surface temperatures can rise above freezing in summer and cause melting, and where fractional cloud cover is typically 80–90% (Lachlan-Cope, 2010). The recent surface temperature rise and the loss of ice mass on more than half of the Peninsula's ice shelves further motivates investigation of cloud in this region (Turner *et al.*, 2005; 2016; Cook and Vaughan, 2010).

Larsen C is the largest remaining ice shelf on the Antarctic Peninsula, occupying $\sim 47,000$ km² (Bevan *et al.*, 2017). Previously neighbouring ice shelves, Larsen A and B, collapsed in 1995 and 2002, respectively, largely as a result of atmospherically driven surface melting (van den Broeke, 2005). Surface melting can destabilise ice shelves via “hydrofracturing”, whereby meltwater percolates into pre-existing rifts and expands, causing crevasses to propagate (Scambos *et al.*, 2000; 2003). Because melt rates are controlled by the balance of surface fluxes, understanding the influence of clouds on the SEB is of great importance to help establish whether Larsen C is likely to suffer the same fate.

Cloud phase strongly influences cloud radiative properties. Mixed-phase clouds dominate in summer over coasts and ice shelves like Larsen C (Lachlan-Cope, 2010; Listowski *et al.*, 2019) and have a complex vertical profile, with multiple thin layers in a “water-over-ice” structure of supercooled liquid droplets above heavier ice crystals (Barrett *et al.*, 2017). Clouds with higher liquid water paths, composed of many small droplets, are less transmissive to incoming short-wave radiation, and more emissive in the infrared, so radiate more long-wave radiation back to the surface (Zhang *et al.*, 1996). However, the vertical position of liquid within the cloud is important: for instance, the supercooled liquid upper layer of mixed-phase clouds can reflect lots of short-wave radiation, but has little effect on long-wave emission (Barrett *et al.*, 2017).

Atmospheric models typically struggle to represent cloud phase or vertical structure correctly, especially at high latitudes. For example, Klein *et al.* (2009) find that models cannot usually simulate enough liquid water in Arctic stratocumulus because too much ice is formed at the

expense of supercooled liquid. Many atmospheric models, including the UK Met Office Unified Model (MetUM) used in this study, exhibit this bias in cloud phase and structure because their microphysical parametrizations are developed for the midlatitudes and are relatively simple. For example, poor representations of processes like riming (Furtado *et al.*, 2016) and vapour deposition (Furtado and Field, 2017), as well as large-scale cloud phase partitioning (Abel *et al.*, 2017) have been shown to cause the MetUM to overestimate cloud ice and underestimate cloud liquid contents. In many models, errors in cloud phase produce significant SEB biases, most notably over the Southern Ocean (Bodas-Salcedo *et al.*, 2012; Hyder *et al.*, 2018). This is because subgrid-scale spatial variability in temperature and humidity are necessarily parametrized in the model by large-scale cloud schemes, which compute liquid and ice cloud fractions that are then fed into the microphysics scheme. In reality, ice and liquid can coexist in spatially segregated pockets (Tan and Storelvmo, 2016), but in the MetUM it is difficult to sustain a separation between the phases. When total cloud fraction exceeds 100%, ice and liquid phases are assumed to overlap within a homogeneously mixed mixed-phase region. In this mixed-phase region, ice forms preferentially because of the lower saturation vapour pressure over ice than liquid.

Modelled cloud has been implicated as a primary driver of surface radiation biases over Antarctica (Bromwich *et al.*, 2013; Lenearts *et al.*, 2017) and specifically over Larsen C (King *et al.*, 2015; Listowski and Lachlan-Cope, 2017). King *et al.* (hereafter K15) find that three different regional atmospheric models simulate either too little cloud, or cloud that is optically too thin over the ice shelf. Summertime clouds over Larsen C in the MetUM are optically too thick in the short-wave part of the spectrum, while being too thin in the infrared, which results in negative downwelling short-wave (SW_{\downarrow}) and long-wave (LW_{\downarrow}) biases. Overall, they find positive (negative) net short-wave (long-wave) fluxes that do not entirely cancel, which produces a positive net energy flux at the surface and can cause the MetUM to overestimate melt on Larsen C. High-resolution regional climate models are typically able to represent the radiative effects of mixed-phase cloud more accurately than global models (Vergara-Temprado *et al.*, 2018). However, computational constraints still necessitate parametrizations that approximate subgrid-scale cloud properties, which produce errors in the SEB. Both Listowski and Lachlan-Cope (2017) and Hines *et al.* (2019) use the Polar-WRF model (and AMPS, in the case of Hines *et al.*) to show that more sophisticated parametrizations produce more accurate simulations of cloud microphysical properties, and consequently surface radiative fluxes, over Larsen C and the West Antarctic, respectively. Both find that double-moment

parametrizations of liquid water represent cloud and SEB properties most accurately.

Over the entire continent, the widely varying representations of cloud phase between models and re-analyses still produce considerable errors in radiative fluxes: generally, CMIP5 models underestimate downwelling short-wave and overestimate downwelling long-wave (Lenaerts *et al.*, 2017). A better understanding of phase in Antarctic mixed-phase clouds, particularly the occurrence of super-cooled liquid water (e.g. Listowski *et al.*, 2019), is essential to address this problem. For example, an improved cloud scheme was shown to reduce Antarctic-wide SEB biases in RACMO2 (Van Wessem *et al.*, 2014), and to increase modelled melt and precipitation rates over the Antarctic Peninsula (Van Wessem *et al.*, 2018). Melt and precipitation are both key inputs to surface mass balance (SMB) calculations, so improving simulated cloud phase and radiative effects contributes to a better understanding of SMB and consequently sea level rise. This is particularly important in coastal Antarctica (including the peninsula), where melt and precipitation rates are high, and model SEB biases are largest (Lenaerts *et al.*, 2017). Antarctic SMB has been estimated using regional models like MAR (Agosta *et al.*, 2018), COSMO-CLM² (Souverijns *et al.*, 2019) and RACMO2 (Lenaerts *et al.*, 2018; Van Wessem *et al.*, 2018), but further work is still required to better constrain modelled SMB. For instance, RACMO2 still overestimates coastal orographic precipitation rates near the grounding line of West Antarctic glaciers partly due to its representation of cloud (Lenaerts *et al.*, 2018).

There is currently a gap in scientific understanding on the influence of cloud phase on the SEB and melting over Antarctic Peninsula ice shelves. This has wider implications for model estimates of SMB across Antarctica, and therefore sea level rise. K15 conclude that cloud properties are a likely cause of observed SEB biases. However, although observed cloud phase on the peninsula has been assessed by Grosvenor *et al.* (2012) and Lachlan-Cope *et al.* (2016) and modelled by Listowski and Lachlan-Cope (2017), no work has been done to explicitly connect these properties to the SEB. This study will address this gap by investigating the sensitivity of the SEB to simulated cloud phase in a high-resolution regional climate configuration of the MetUM.

2 | DATA AND METHODS

2.1 | Study area

The study focuses on Larsen C, an ice shelf with a flat, homogenous surface on the eastern side of the mountains that extend approximately north–south along the

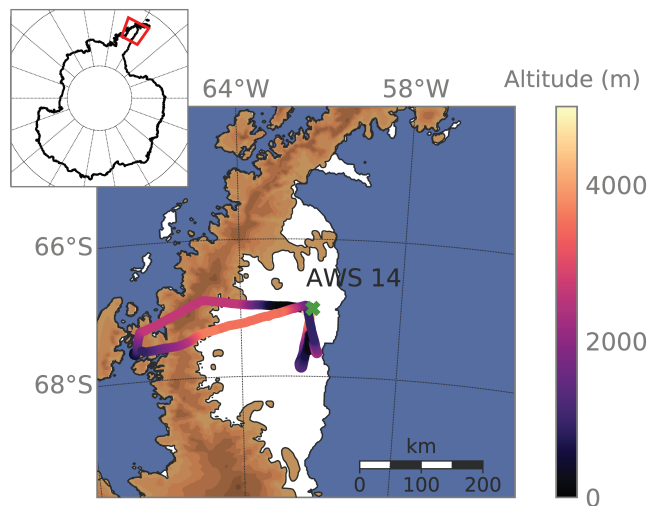


FIGURE 1 The inner 1.5 km resolution MetUM model domain used in this study, centred on Larsen C ice shelf. The model's surface elevation is indicated by shaded contours. The flight track of the f152 case-study is also shown, where the aircraft's altitude is indicated by the scale shown on the right, and the location of AWS14 is marked with a cross. The inset map shows the location of the model domain in a wider Antarctic context

Antarctic Peninsula (Figure 1). During summer, the shelf is characterised by relatively low wind speeds, high relative humidity and cloudy conditions (Kuipers Munneke *et al.*, 2012).

2.2 | Data

Two observational datasets are used to validate MetUM-simulated cloud phase and SEB over Larsen C, namely, airborne observations of cloud collected with the British Antarctic Survey's instrumented Twin Otter aircraft and observations of surface meteorology and energy fluxes from an automatic weather station (AWS14), located at 67°00.8'S 61°28.8'W at 40 m above sea level. These data are from the Orographic Flows and Climate of the Antarctic Peninsula (OFCAP) campaign which took place between 1 January and 7 February 2011 (Elvidge *et al.*, 2015; 2016; K15).

The aircraft measures standard meteorological variables like temperature, pressure and humidity, three-dimensional winds and up- and downwelling radiation. A DMT Cloud, Aerosol and Precipitation Spectrometer (CAPS probe: Baumgardner *et al.*, 2001) containing three separate instruments to sample cloud particles of different sizes was also fitted. A full description of aircraft observations and data treatment can be found in Grosvenor *et al.* (2012), Lachlan-Cope *et al.* (2016) and Appendix A.

AWS14 measures near-surface meteorology and radiation components directly. Turbulent fluxes are computed using the bulk aerodynamic method to retrieve the full SEB, and the energy balance model of van den Broeke *et al.* (2005) calculates the SEB of the snowpack. Further details of weather station measurements and data treatment are given in Kuipers Munneke *et al.* (2009; 2012) and Appendix B.

The SEB of the ice surface is defined as per K15 and summarised as:

$$E_{\text{tot}} = SW_{\text{net}} + LW_{\text{net}} + H_L + H_S, \quad (1)$$

where SW_{net} and LW_{net} are the net (downwelling minus upwelling) short-wave and long-wave fluxes, respectively; and H_L and H_S are the surface latent and sensible heat fluxes, respectively. Melting occurs when the sum of fluxes, E_{tot} , is positive, and the surface temperature, T_s , is at the melting point: 0°C . Energy available for melting (or melt flux, E_{melt}) is therefore equal to E_{tot} when $T_s = 0^\circ\text{C}$, as described in K15. All fluxes, including E_{melt} and E_{tot} , are measured in $\text{W}\cdot\text{m}^{-2}$ and are positive when directed towards the surface.

2.3 | Model description

The MetUM (Walters *et al.*, 2017) is a non-hydrostatic numerical weather prediction model that uses semi-implicit time-stepping and semi-Lagrangian advection. A regional configuration using RA1 science settings was run in atmosphere-only forecast mode, with a set-up adapted from Orr *et al.* (2014) and forecast length of 24 hours. It was run in a nested configuration with a 1.5 km resolution inner domain centred on the Larsen C ice shelf, shown in Figure 1. This domain is positioned within a global domain that has ~ 17 km resolution at midlatitudes (N768) and was initialised with global UK Met Office operational analyses. The MetUM radiation scheme is based on Edwards and Slingo (1996) and all experiments used the operational single-moment cloud microphysics scheme based on Wilson and Ballard (1999), with extensive modifications as described in Bush *et al.* (2019). The heterogeneous ice nucleation temperature threshold (representing an immersion freezing or condensation mechanism, whereby ice is permitted to form heterogeneously in the presence of liquid water) used by the microphysics scheme was changed from its default value of -10°C to -18°C , shown by Field *et al.* (2014) to improve the representation of mixed-phase cloud. Additional details of model parametrizations are given in Appendix C.

2.4 | Method

Cloud properties and surface fluxes are examined in detail during one instructive case-study (flight 152, hereafter referred to as f152, conducted on 18 January 2011). This flight was selected because the aircraft conducted two vertical profiles between 100 and 5,000 m near AWS14. The flight track and location of AWS14 are shown in Figure 1. Observed and modelled surface fluxes and in-cloud vertical profiles are compared at AWS14 during f152. Model output is taken from the closest grid point to AWS14's location, plus the eight surrounding grid points: an area of approximately 4.5 km^2 . Because AWS14 is located on a flat, homogeneous ice surface, it can be reasonably assumed that conditions there are representative of a large area (K15). Mean vertical profiles are computed from observations and model output using in-cloud data only, during the period when the aircraft was sampling over the ice shelf (approximately 1500–1700 UTC). Further detail is given in the appendices.

Four model experiments were run with varying ‘‘Regional Atmosphere’’ (RA) configurations (Table 1). Two sets of RA physics were tested: RA1M and RA1T, configured for the midlatitudes and Tropics, respectively, and described in Bush *et al.* (2019). These two experiments are the ‘‘base’’ configurations. The primary differences between them is that RA1M uses the operational (diagnostic) large-scale cloud scheme based on Smith (1990), whereas RA1T uses a prognostic scheme, PC2 (Wilson *et al.*, 2008). Smith (1990) parametrizes subgrid-scale variations in humidity and temperature to calculate cloud fractions using a triangular probability distribution function. Condensation within a grid box occurs when relative humidity reaches a critical value, RH_{crit} , which is specified for each model layer. Cloud liquid and ice fractions (that is, the fraction of the grid box occupied by liquid or ice cloud) are calculated by the scheme from the liquid and ice contents, before this information is fed into the microphysics for further calculation of cloud properties. The PC2 scheme is prognostic and computes liquid, ice and mixed-phase cloud fractions, which are advected in space and time after updating them by calculating sources and sinks of condensate. Incremental condensate fractions are outputted following each physical process represented by the model, such that each scheme (convection, radiation etc.) must produce an effect on condensate fractions. The connection to the microphysics scheme is slightly adapted compared to Smith (1990), so that autoconversion does not affect liquid cloud fractions. In practice, this permits the existence of extensive, optically thin liquid clouds, with high liquid cloud fraction but low liquid water contents.

TABLE 1 Configurations for model experiments used in this study

Experiment name	Options
RA1M	<ul style="list-style-type: none"> • RA1M physics, based on Smith (1990) large-scale cloud scheme • Heterogeneous nucleation temperature threshold set to -18°C (Field <i>et al.</i>, 2014)
RA1M_mod	As in RA1M, with the following modifications: <ul style="list-style-type: none"> • Shape-dependent riming (Furtado and Field, 2017) • Modified ice cloud fraction parametrization (Abel <i>et al.</i>, 2017)
RA1T	<ul style="list-style-type: none"> • RA1T physics, based on PC2 (Wilson <i>et al.</i>, 2008) large-scale cloud scheme • Heterogeneous nucleation temperature threshold set to -18°C (Field <i>et al.</i>, 2014)
RA1T_mod	As in RA1T, with the following modifications: <ul style="list-style-type: none"> • Turbulent production of supercooled water (Furtado <i>et al.</i>, 2016) • Shape-dependent riming (Furtado and Field, 2017)

The second two experiments (RA1M_mod and RA1T_mod) applied modifications to the base configurations shown to improve the simulation of cold mixed-phase clouds by increasing the supply of liquid water and reducing its conversion to ice (see Table 1 for a summary). These are: (a) the inclusion of shape-dependent riming (Furtado and Field, 2017), (b) the turbulent production of supercooled liquid (Furtado *et al.*, 2016, RA1T only), and (c) modifications to the ice cloud fraction parametrization described in Abel *et al.* (2017) (RA1M only). Firstly, riming depletes liquid water, so limiting the efficiency of this process can sustain higher liquid fractions in mixed-phase clouds. Reducing riming efficiency has been shown to improve Southern Ocean downwelling short-wave radiation biases associated with the conversion of too much cloud liquid water to ice (Furtado and Field, 2017). Secondly, cloud liquid water can also be produced by subgrid-scale variations in humidity that are related to unresolved turbulence. Because turbulent motions occur at finer scale than the MetUM can explicitly resolve, this can produce humidity distribution differences that are also not directly simulated. Furtado *et al.* (2016) demonstrated that increasing the supply of liquid in this manner can enhance the amount of cloud liquid. This modification is only compatible with the PC2 cloud scheme, on which RA1T is based. Finally, several studies show that ice cloud fractions are consistently overestimated in mixed-phase clouds by the MetUM (e.g. Field *et al.*, 2014; Abel *et al.*, 2017) due to computational limitations that mean that the model cannot explicitly resolve small-scale spatial heterogeneity in cloud water phase. Abel *et al.* (2017) develop an adaptation to the ice cloud fraction parametrization that limits the overlap between the liquid and ice fractions, thereby reducing the conversion of liquid to ice via vapour deposition and riming. This adaption mimics the real-world existence of spatially discrete (subgrid-scale) pockets of ice and liquid without explicitly resolving them. It is only compatible with the RA1M scheme.

The case-study was simulated with all four model configurations, then the best-performing configuration was used to simulate the entire five-week OFCAP period. During OFCAP, only the representation of surface fluxes is assessed because cloud phase measurements are not consistently available throughout the period. Initial tests showed modelled cloud phase to be sensitive to forecast length, so the first 12 hr of each 24 hr forecast were discarded as spin-up. The case-study simulation was initialised at 0000 UTC on 18 January 2011 to allow the model to spin up. For the longer OFCAP simulation, forecasts were re-initialised every 12 hr and the $t + 12$ to $t + 24$ hr part of each successive forecast was concatenated to form a continuous time series.

3 | RESULTS AND DISCUSSION

3.1 | Model representation of case-study f152

Observed ice and liquid mass mixing ratios during case f152 (18 January 2011) over AWS14 indicate that many thin cloud layers are present, with clouds below 2 km exhibiting the “water-over-ice” structure typical of low-level polar mixed-phase clouds (Figure 2). A higher altostratus layer is present at around 4 km altitude, while a stratocumulus deck is observed between approximately 400 and 2,200 m. This stratocumulus appears in two distinct layers and contains higher mass mixing ratios of cloud ice and liquid than the upper-level altostratus, reaching $1.6 \times 10^{-2} \text{ g}\cdot\text{kg}^{-1}$ and $3.4 \times 10^{-1} \text{ g}\cdot\text{kg}^{-1}$, respectively. While the MetUM successfully captures the presence of altostratus and lower stratocumulus layers, all four model configurations simulate the lowest cloud layer around 1 km higher than is observed and produce just one layer below 2 km rather than the two indicated by the observations.

FIGURE 2 Mean vertical profiles of cloud (a) ice and (b) liquid mass mixing ratios, in $\text{g}\cdot\text{kg}^{-1}$, and mean modelled cloud grid-box volume fractions of (c) ice cloud and (d) liquid cloud during fl52 when the aircraft was sampling over Larsen C. Observations are shown in (a) and (b) with the solid black line and model output above AWS14 is shown in all panels by lines with markers. Solid lines with heavy markers indicate the two “base” configurations, while dashed lines with lighter markers show their modified counterparts. The experimental configurations are detailed in Table 1

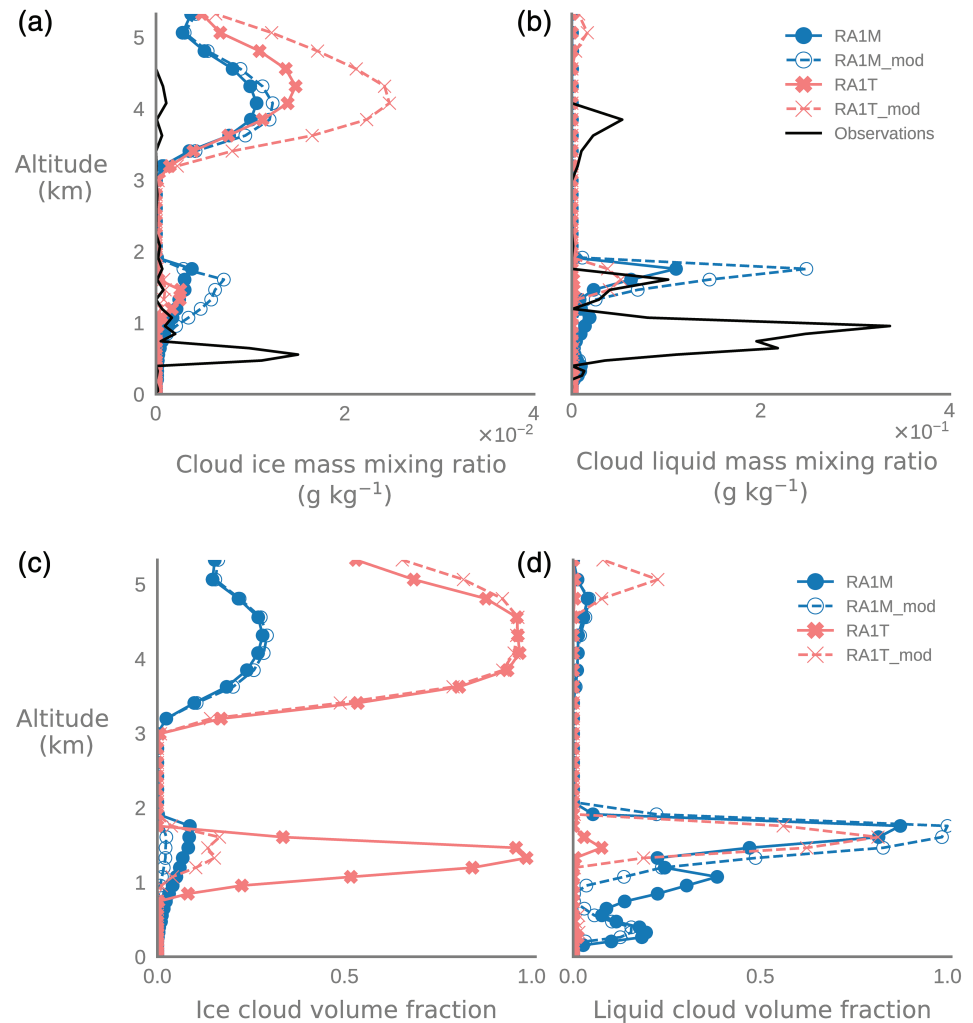


Figure 2 shows that all model configurations (RA1M, RA1M_mod, RA1T and RA1T_mod) overestimate ice mass mixing ratios, and underestimate liquid mass mixing ratios above 2.5 km altitude, where virtually no liquid is present in any configuration. Ice cloud is concentrated in the upper layers (above ~ 3 km) because any supercooled liquid present is converted readily to ice below the ice nucleation temperature threshold of -18 °C. At 4 km altitude, the largest positive bias in ice contents is in RA1T_mod, which produces an ice mass mixing ratio 22.7 times larger than observed, while RA1M shows the smallest bias: an overestimate of 2.3 times. All models except RA1T_mod produce liquid mass mixing ratios of less than $5.0 \times 10^{-4} \text{ g}\cdot\text{kg}^{-1}$ above 4 km, although liquid mixing ratios are observed to reach $5.3 \times 10^{-2} \text{ g}\cdot\text{kg}^{-1}$ at 3.8 km. At lower altitudes modelled cloud generally contains less liquid and ice than observed. Between 1 and 2 km, ice mass mixing ratios in RA1M_mod peak at $7.2 \times 10^{-3} \text{ g}\cdot\text{kg}^{-1}$, 1.9 times higher than RA1M, and 2.8 and 7.5 times larger than in RA1T and RA1T_mod, respectively. At the same height, liquid mass mixing ratios peak in RA1M and RA1M_mod

at $1.1 \times 10^{-1} \text{ g}\cdot\text{kg}^{-1}$ and $2.5 \times 10^{-1} \text{ g}\cdot\text{kg}^{-1}$, respectively, and at $2.1 \times 10^{-3} \text{ g}\cdot\text{kg}^{-1}$ and $5.2 \times 10^{-2} \text{ g}\cdot\text{kg}^{-1}$ respectively in RA1T and RA1T_mod. Overall, ice mass mixing ratios are overestimated (by between 1.7 times in RA1M and 5.1 times in RA1T_mod), while liquid mass mixing ratios are underestimated (by 3.0 times in RA1M_mod to 64.9 times in RA1T). This is consistent with the results of Furtado *et al.* (2016) and Abel *et al.* (2017) who find that riming and vapour deposition occur too efficiently in modelled cold mixed-phase clouds, forming ice too readily at the expense of supercooled liquid.

The midlatitude configuration of the model, RA1M, simulates cloud ice and liquid mass mixing ratios that are closer to those observed than the tropical configuration, RA1T. RA1T produces little liquid cloud compared to observations, evident from Figure 2b, and compared to RA1M, shown in Figure 2b,d. Additionally, RA1T only simulates thin ice clouds over AWS14. This is suggested by Figure 2c, which shows that ice cloud volume fraction reaches 100% at 1.2 km, and Figure 2a, which shows very low ice mass mixing ratios in this layer.

Modelled “volume fractions” refer to the fraction of a grid box occupied by cloud of each phase; volume fractions in Figure 2 are shown as means for each model layer. RA1T is designed for use in tropical, convective regions and is less suited to Antarctic conditions where convection is less vigorous, which may explain these differences.

Modifications to the “base” model configurations produce varying results. Observed liquid mass fractions in the lowest simulated cloud layer peak at $3.4 \times 10^{-1} \text{ g} \cdot \text{kg}^{-1}$. At $2.5 \times 10^{-1} \text{ g} \cdot \text{kg}^{-1}$, RA1M_mod produces 2.3 times more liquid than RA1M in the lowest layer, but the modifications to RA1M do not change its height, which is still approximately 1 km too high in RA1M_mod. RA1T_mod generates 1.7 times more cloud ice above 3 km than RA1T, but is the only configuration to simulate liquid at this height, as is observed (Figure 2d). Throughout the profile, it also produces almost 10 times as much liquid than RA1T, but liquid mass fractions in RA1T_mod are still around six times lower than in observations. Of all four experiments, RA1M_mod exhibits the lowest bias in liquid mass fractions, while RA1M overestimates ice mass fractions by the smallest amount.

Specific humidity, that is, water vapour mass fraction, is represented reasonably accurately (within 10–25% of observed values) in all experiments throughout the profile up to 2 km (not shown). However, between 2 and 3.5 km, modelled water vapour mass fractions are considerably lower than observed (by 63–65% at 2.6 km). This underestimation of water vapour may be expected to negatively bias long-wave fluxes. However, very few differences are detectable between configurations, so this effect should have the same effect on the SEB in all experiments.

Surface flux biases at AWS14 for each model experiment during f152 are presented in Table 2. Energy available for melting, E_{melt} , is overestimated by all configurations of the MetUM, but the bias is highest in RA1M at $17.33 \text{ W} \cdot \text{m}^{-2}$, causing modelled E_{melt} to be too large by 37%. Because the modelled and observed surface temperature are at melting point throughout the flight (not shown), this bias is solely driven by errors in the simulated surface fluxes. Additionally, the modelled surface albedo ($SW_{\uparrow} / SW_{\downarrow}$) is within $\pm 2\%$ of observed values in all simulations, suggesting that biases are driven almost entirely by downwelling radiative errors, and highlighting the importance of cloud phase in determining melt. Net short-wave fluxes (SW_{net}) are simulated better by the two midlatitude experiments, with the lowest bias produced by RA1M_mod ($-1.80 \text{ W} \cdot \text{m}^{-2}$), while the smallest bias in net long-wave ($-4.68 \text{ W} \cdot \text{m}^{-2}$) is found in RA1T_mod. Both modified experiments produce lower short-wave flux biases than their respective “base” configurations,

but RA1M produces smaller LW_{\downarrow} and LW_{net} biases than RA1M_mod.

Between-experiment differences in downwelling fluxes are partly driven by the representation of cloud. Positive SW_{\downarrow} biases in all experiments indicate that the cloud is optically too thin in this part of the spectrum, thus allowing too much solar radiation to reach the surface (as also found by K15). Conversely, overestimated LW_{\downarrow} indicates that the cloud is optically too thick in the infrared, which can be related to cloud liquid water content, temperature or altitude (Zhang *et al.*, 1996). The lowest simulated cloud layer is approximately 1 km too high in all experiments, while temperature profiles are represented well compared to observations (not shown). A higher cloud base would be expected to contribute to negative LW_{\downarrow} and LW_{net} biases in all experiments, but this is only true of the two RA1T experiments, suggesting a role for other effects, such as biases in parametrized cloud particle size. RA1T_mod exhibits the smallest LW_{\downarrow} bias, while RA1T has the largest. LW_{\downarrow} biases are positive in the two RA1M experiments, and negative in the RA1T experiments, although LW_{\downarrow} and LW_{\uparrow} biases are both comparatively small in RA1T_mod. Positive LW_{\downarrow} biases in RA1M and RA1M_mod are also likely a result of errors in simulated cloud phase, which are only partly offset by negative water vapour biases (not shown). Thick ice clouds can have a significant long-wave warming effect (Miller *et al.*, 2015), so although specific humidity and liquid contents – usually the dominant component of cloud long-wave radiative forcing – are underestimated, the considerable overestimation of ice contents at altitudes above 3 km likely explains this positive bias.

The RA1T experiment produces quite different cloud profiles, and consequently SEB biases, to the other three simulations. As shown in Figure 2, RA1T produces very low liquid cloud fractions and virtually no liquid water throughout the cloud profile, which likely explains the negative LW_{\downarrow} ($-41.13 \text{ W} \cdot \text{m}^{-2}$) and extremely positive SW_{\downarrow} ($195.38 \text{ W} \cdot \text{m}^{-2}$) biases shown in Table 2. The amount of short-wave radiation transmitted through ice clouds is relatively insensitive to ice cloud thickness (Miller *et al.*, 2015), which means that although RA1T simulates an ice cloud grid-box volume fraction of 100% in two layers (Figure 1c,d), this has a limited effect on surface SW_{\downarrow} because solar radiation can still penetrate. RA1T produces a melt flux bias comparable to RA1M_mod because its large radiative biases cancel and biases in the turbulent fluxes are relatively minor.

RA1T_mod has the smallest LW_{\downarrow} bias, but this may be due to errors in simulated cloud phase. A positive SW_{\downarrow} bias indicates that too little (liquid) cloud is simulated (also suggested by the low liquid water contents and volume fractions in Figure 2), which would usually be associated

TABLE 2 Time mean observed surface energy fluxes and model biases of each experiment at AWS14 during f152

	AWS14 (observed)	Mean bias			
		RA1M	RA1M_mod	RA1T	RA1T_mod
SW_{\downarrow}	594.58	66.14	30.26	195.38	114.84
SW_{\uparrow}	-501.34	-55.39	-32.06	-135.05	-84.90
SW_{net}	93.24	10.73	-1.80	60.33	29.95
LW_{\downarrow}	279.11	9.21	12.37	-41.13	-5.11
LW_{\uparrow}	-315.64	0.28	0.25	0.79	0.43
LW_{net}	-36.53	9.50	12.63	-40.34	-4.68
H_S	-3.63	-2.37	-3.49	-8.62	-6.62
H_L	-10.85	7.78	7.87	1.40	6.21
E_{tot}	42.23	25.05	13.15	15.29	23.35
E_{melt}	47.31	17.33	6.09	9.63	16.52

All fluxes are given in $\text{W}\cdot\text{m}^{-2}$, and are abbreviated as in Equation 1. Fluxes and biases are positive when directed towards the surface. The smallest biases are highlighted in bold text.

with a large negative LW_{\downarrow} bias. However, cloud occupies up to 80% of the grid box in the lowest layer, despite the liquid water contents being far too low, suggesting that the layer is extremely thin. Optically thin liquid clouds have been shown to cause greater warming than thicker liquid clouds in summer over the Greenland ice sheet because they are thin enough to allow short-wave radiation to penetrate, but thick, low and warm enough to radiate strongly in the infrared (Bennartz *et al.*, 2013). Errors in simulated cloud phase may therefore produce small biases for the wrong reasons.

Overall, RA1M_mod is considered to be the best-performing experimental configuration with respect to cloud and SEB properties. Erroneous cloud fields and large cancelling radiative flux errors remove RA1T and RA1T_mod from consideration. RA1M and RA1M_mod have comparable net long-wave biases, and although cancelling SW_{\downarrow} and SW_{\uparrow} errors exist in both, these are smaller in RA1M_mod, which overestimates SW_{\downarrow} by just 5%. Further, RA1M_mod's E_{tot} and E_{melt} biases are the smallest of all configurations. RA1M_mod is therefore used to run a five-week simulation of the OFCAP period for a second evaluation of simulation quality.

3.2 | Model representation of the OFCAP period

Errors in cloud phase have been shown to contribute to errors in downwelling fluxes during flight 152. However, because aircraft observations of cloud properties are not available for the entire period, a similar analysis is not possible for OFCAP. Downwelling fluxes are therefore used to infer information about cloud phase

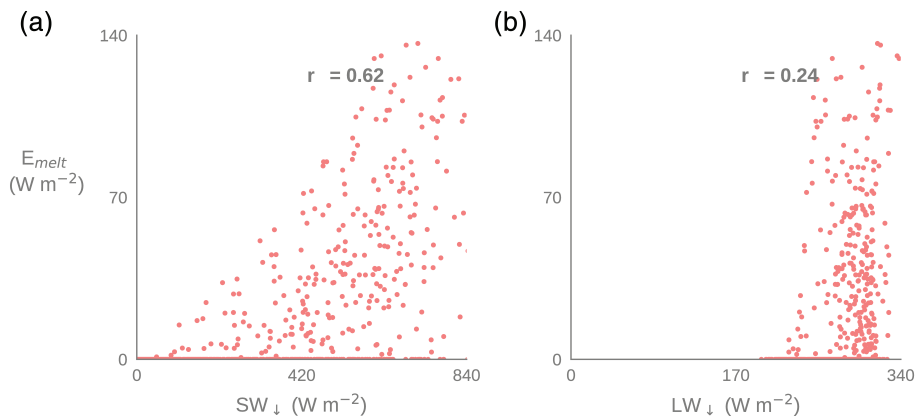
during OFCAP. Pearson correlation coefficients are used to understand relationships between melting and observed fluxes (Table 3, Figure 3).

Table 3a and Figure 3 show positive correlations (significant at the 99% level) between observed E_{melt} and SW_{\downarrow} ($r_{\text{SW,melt}} = 0.62$, Figure 3a) and LW_{\downarrow} ($r_{\text{LW,melt}} = 0.24$, Figure 3b). This indicates that melt is most likely to occur when more short-wave radiation can reach the surface, but is also weakly associated with higher LW_{\downarrow} , which is strongly related to liquid water contents, especially at the relatively low liquid water paths ($<40 \text{ g}\cdot\text{m}^{-2}$) typical of Antarctic clouds (Grosvenor *et al.*, 2017). Observed melt is not strongly related to cloud cover ($r_{\text{CC,melt}} = 0.12$), where “cloud cover” is defined as the portion of the sky above AWS14 occupied by cloud, and the negative correlation between SW_{\downarrow} and cloud cover shows that SW_{\downarrow} is highest during clear conditions ($r_{\text{CC,SW}} = -0.19$), which occur 11.5% of the time (defining “clear” as having cloud cover <0.31 , as in Kay *et al.* (2008)). The low observed correlation between cloud cover and melt may be explained by the competing effects of cloud long-wave (positive correlation) and short-wave (negative correlation) radiative effects on melt. Observed cloud cover is not compared with LW_{\downarrow} because it is computed from the closure of the long-wave radiation budget using the energy balance model of Kuipers Munneke *et al.* (2009) and so is not independent. Modelled relationships (Table 3b) compare well with observations, suggesting that the model is able to reproduce the observed drivers of melting. For example, modelled E_{melt} is positively correlated with SW_{\downarrow} ($r_{\text{SW,melt}} = 0.65$) and to a much lesser extent, LW_{\downarrow} ($r_{\text{LW,melt}} = 0.15$). Additionally, the large and significant (at the 99% level) correlation between modelled cloud cover and LW_{\downarrow} ($r_{\text{CC,LW}} = 0.87$) suggests that cloud cover affects

TABLE 3 Pearson correlation coefficients between cloud cover, downwelling long-wave (LW_{\downarrow}) and short-wave fluxes (SW_{\downarrow}), and melt flux, (E_{melt}), at AWS14 during 1 January–7 February 2011

	(a) Observed correlations				(b) Modelled correlations			
	Cloud cover	LW_{\downarrow}	SW_{\downarrow}	E_{melt}	Cloud cover	LW_{\downarrow}	SW_{\downarrow}	E_{melt}
Cloud cover	1.00	—	-0.19	0.12	1.00	0.87	-0.14	0.05
LW_{\downarrow}		1.00	—	0.24	1.00	—		0.15
SW_{\downarrow}			1.00	0.62			1.00	0.65
E_{melt}				1.00				1.00

Correlation coefficients between observed components are shown in panel (a), while modelled coefficients are given in panel (b). Correlation coefficients in bold text are significant at the 99% level.

**FIGURE 3** Scatterplots of observed energy available for melting (E_{melt}) against (a) downwelling short-wave (SW_{\downarrow}) and (b) downwelling long-wave (LW_{\downarrow}) at AWS14. Data plotted are instantaneous values outputted at 30 min intervals. Pearson correlation coefficients, significant at the 99% level, are given at top centre of each panel

long-wave fluxes most strongly in the MetUM. This is mostly due to the contribution of liquid clouds – the correlation between LW_{\downarrow} and liquid water path is much higher ($r_{\text{LWP, LW}} = 0.63$) than with ice water path ($r_{\text{IWP, LW}} = 0.21$) (not shown). Modelled melting during OFCAP usually follows cloudy periods, during which liquid and then ice water paths increase and then rapidly decline as cloud glaciates and dissipates (not shown). Higher cloud liquid water contents increase LW_{\downarrow} and begin to increase surface temperature and E_{tot} . Melting first begins as LW_{\downarrow} increases, but is then sustained as the cloud glaciates and more short-wave radiation can reach the surface. This time-evolving process may partly explain the relatively low modelled correlations with melt of cloud cover and downwelling fluxes.

Biases in modelled SEB terms during the OFCAP period (Table 4) are smaller than those reported by K15, who use an earlier version of the default MetUM configuration, and broadly similar to those during f152 (Table 2). As in f152, SW_{net} is negatively biased, but not for the same reasons: whereas during f152 SW_{\downarrow} is positively biased, during OFCAP it is negatively biased, indicating that cloud is optically too thick in the short-wave part of the spectrum during the OFCAP period. This finding is consistent with K15. Mean long-wave biases are

all $\sim 1 \text{ W}\cdot\text{m}^{-2}$ in magnitude, but LW_{\downarrow} (and consequently LW_{net}) shows a poor correlation with observations, indicating that the model struggles to represent (liquid) clouds, atmospheric water vapour contents and/or that clouds are simulated at the wrong time. This is consistent with results from the case-study, which shows that the MetUM represents some cloud properties poorly. For example, errors in simulated cloud base height may explain the poor correlation with observed LW_{\downarrow} , as seen for the f152 case, when the MetUM-simulated cloud base was 1 km too high.

As shown in Table 4, modelled radiative biases during OFCAP are mostly of the same sign as K15, but smaller in magnitude, suggesting that the MetUM physics updates since 2015 and modifications made in this work have improved the representation of cloud microphysics, and consequently surface energy fluxes. The melt flux bias is smaller than in K15 and during f152 ($-1.7 \text{ W}\cdot\text{m}^{-2}$ compared to $7.6 \text{ W}\cdot\text{m}^{-2}$ in K15 and $6.09 \text{ W}\cdot\text{m}^{-2}$ in f152, an underestimate of just 12%), but of the opposite sign. This results in a 13% underestimate of cumulative meltwater production throughout OFCAP, at 114 mm (water equivalent). K15 found that the MetUM overpredicts the occurrence of melt, despite a cold bias that is particularly present at high latitudes where conditions are more stable (Lock,

TABLE 4 Mean observed surface energy fluxes at AWS14 and mean model biases of each experiment during the OFCAP period, as in Table 2

	AWS14 (observed)	Mean bias			Correlation coefficient
		K15	RA1M_mod	RMSE	
SW_{\downarrow}	277.86	-31.6	-20.95	105.03	0.91
SW_{\uparrow}	-232.69	41.0	12.78	87.78	0.91
SW_{net}	45.17	9.4	-8.16	24.88	0.85
LW_{\downarrow}	280.10	-7.0	-0.33	33.01	0.49
LW_{\uparrow}	-303.88	-2.0	1.17	14.12	0.63
LW_{net}	-23.79	-6.3	0.84	25.70	0.47
H_L	-5.11	1.9	4.59	8.70	0.71
H_S	-9.34	5.9	6.35	11.46	0.48
E_{tot}	-1.43	10.5	11.98	31.71	0.78
E_{melt}	13.53	7.6	-1.72	16.26	0.82

Mean biases reported by K15 are given in the third column, and mean biases, root-mean-square errors and Pearson correlation coefficients of the OFCAP simulation are given in columns four to six. As in Table 2, the smallest biases are highlighted in bold, and fluxes and biases are positive when directed towards the surface.

2011). Although the OFCAP simulation also produces a small mean cold bias (-0.27°C), and exhibits considerable negative biases in surface temperature during night-time, it represents melt frequency well because errors in modelled surface temperature are mostly when it is already well below the melting point (Figure 4). Observed melting occurs 29.5% of the time during OFCAP, while the model simulates melting 32% of the time. E_{melt} biases are therefore smaller than E_{tot} biases because melt occurs only when the surface temperature is at melting point. Remaining biases, for instance in the turbulent fluxes, may be explained by other sources of error, such as the land surface or boundary-layer schemes. Improvements made in the RA1M_mod configuration produce much better simulations of melt at AWS14 than the present default configurations and previous model versions. Because surface fluxes at AWS14 are representative of a wider area (K15) and the large-scale meteorological forcing producing cloud is similar across the ice shelf, these improvements will likely be seen across the whole of Larsen C.

4 | CONCLUSIONS

This study has shown that the representation of cloud phase in the MetUM strongly influences modelled summertime surface energy fluxes and melt over the Larsen C ice shelf. An optimum configuration, RA1M_mod, is identified and recommended for future work examining cloud properties and surface energy fluxes over the Antarctic

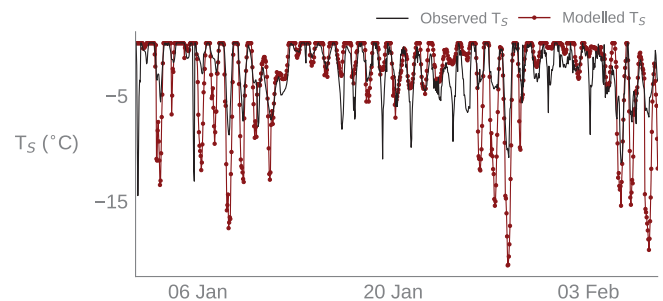


FIGURE 4 Hourly surface temperature (T_s) at AWS14 during the OFCAP period. Observations are given in black, while model output is shown with filled markers

Peninsula. RA1M_mod uses single-moment microphysics and is based on the MetUM's midlatitude regional atmosphere package, including modifications proposed by Furtado and Field (2017) and Abel *et al.* (2017). These adaptations to improve simulated cloud phase have wider applications for other regional models and in other regions of Antarctica.

Visual inspection of vertical cloud profiles during a case-study suggests that RA1M_mod reproduces the observed cloud vertical structure most closely. All model configurations overestimate ice concentrations in a mid-level altostratus layer (between ~ 3 and 5 km) and underestimate liquid concentrations throughout the atmosphere, although this is especially visible at lower levels (below ~ 2 km). RA1M_mod produces the second lowest ice mass mixing ratios above 3 km and twice as

much liquid as the next-best configuration in a lower layer, bringing the modelled cloud liquid mass mixing ratio closer to observed values.

By improving the MetUM's representation of cloud phase in a case-study, RA1M_mod restricts biases in downwelling radiative fluxes to around 5% of their observed values. The resultant net radiation bias of $10.83 \text{ W}\cdot\text{m}^{-2}$ is almost half that of $20.23 \text{ W}\cdot\text{m}^{-2}$ produced by the default RA1M configuration. During the whole OFCAP period, only the model's representation of surface fluxes was evaluated because continuous observations of cloud properties were not available. Biases in downwelling radiative fluxes during the OFCAP period were less than 8% of their observed values, which produced a net radiation bias of $-7.32 \text{ W}\cdot\text{m}^{-2}$ (11%). RA1M_mod is able to simulate the occurrence and magnitude of summertime melt better than the versions of the MetUM used in previous studies, such as K15, which used the default Smith (1990) large-scale cloud scheme without the modifications noted here. Over the entire OFCAP period, we find a mean bias of $-1.72 \text{ W}\cdot\text{m}^{-2}$ in modelled melt flux at AWS14, which represents a four-fold reduction on the bias of $7.6 \text{ W}\cdot\text{m}^{-2}$ reported by K15. Despite this improvement, further developments in the representation of cloud phase are evidently still needed to reduce summertime biases in melt. Observed cumulative meltwater production of 114 mm (water equivalent) during the OFCAP period is still underestimated by 13% due to errors in the modelled SEB. Biases of 4.59 and $6.35 \text{ W}\cdot\text{m}^{-2}$ in the latent and sensible heat fluxes, respectively, account for a large proportion of the overall biases in E_{tot} and are greater than those shown in K15. Remaining sources of error likely include model schemes beyond the scope of this article, such as the land surface, snow or boundary-layer schemes.

The RA1M set-up likely outperforms the RA1T configurations because it has been more extensively developed, and is designed for use in colder midlatitude conditions, that are more comparable to those observed in the Antarctic, and because it is based on the Smith (1990) large-scale cloud scheme, which has been more extensively modified and tested than the prognostic PC2 scheme on which RA1T is based. RA1T probably requires further development before it is suitable for use in the Antarctic environment. Additionally, the superior performance of RA1M_mod over the basic RA1M set-up supports the findings of previous work that modifications to increase the amount of liquid and limit its conversion to ice improve the representation of cold mixed-phase clouds (Furtado and Field, 2017; Abel *et al.* 2017). These modifications may also be compatible with the MetUM's double-moment microphysics scheme, which is currently

in development, although this requires further investigation. The RA1M_mod configuration will improve simulations of surface melting and ice shelf change in this rapidly changing environment, and, in future work, we will use RA1M_mod to produce a multi-decadal hindcast to investigate atmospheric processes influencing the SEB and hence melting of Antarctic Peninsula ice shelves.

ACKNOWLEDGEMENTS

The authors confirm that they have no conflicts of interest to declare. This work was supported by the Natural Environment Research Council through the EnvEast Doctoral Training Partnership (grant number NE/L002582/1). The authors also acknowledge use of the MONSOON system, a collaborative facility supplied under the Joint Weather and Climate Research Programme, a strategic partnership between the Met Office and the Natural Environment Research Council. The authors gratefully acknowledge the comments of two anonymous reviewers, which considerably strengthened the study.

DATA AVAILABILITY STATEMENT

Model data are available from the UK Met Office Managed Archive Storage System (MASS). AWS data can be retrieved from <https://www.projects.science.uu.nl/iceclimate/aws/>. Aircraft data are available from the British Atmospheric Data Centre, which can be cited as: Natural Environment Research Council; Lachlan-Cope, T.; Elvidge, A.D.; Smith, V.; Kirchgassner, A.; King, J.C.; Ladkin, R. (2014): British Antarctic Survey Twin Otter aircraft Meteorological Airborne Science INSTRUMENTATION (MASIN) core data from the Orographic Flows and the Climate of the Antarctic Peninsula (OCAF) project (2011). NCAS British Atmospheric Data Centre, 24 September 2014. doi:10.5285/2f53b18d-49fc-4477-b994-f1719d6f6d6e.

ORCID

E. Gilbert  <https://orcid.org/0000-0001-5272-8894>

I. A. Renfrew  <https://orcid.org/0000-0001-9379-8215>

REFERENCES

- Abel, S.J., Boutle, I.A., Waite, K., Fox, S., Brown, P.R.A., Cotton, R., Lloyd, G., Choullarton, T.W. and Bower, K.N. (2017) The role of precipitation in controlling the transition from stratocumulus to cumulus clouds in a Northern Hemisphere cold-air outbreak. *Journal of the Atmospheric Sciences*, 74(7), 2293–2314. <https://doi.org/10.1175/JAS-D-16-0362.1>.
- Agosta, C., Amory, C., Kittel, C., Orsi, A., Favier, V., Gallée, H., van den Broeke, M.R., Lenaerts, J.T.M., van Wessem, J.M. and Fetweis, X. (2018) Estimation of the Antarctic surface mass balance

- using the regional climate model MAR (1979–2015) and identification of dominant processes. *The Cryosphere Discussions* 2018, (D), 1–22. <https://doi.org/10.5194/tc-2018-76>.
- Baran, A.J., Hill, P., Furtado, K., Field, P. and Manners, J. (2016) A coupled cloud physics–radiation parameterization of the bulk optical properties of cirrus and its impact on the Met Office Unified Model Global Atmosphere 5.0 configuration. *Journal of Climate*, 27(20), 7725–7752. <https://doi.org/10.1175/JCLI-D-13-00700.1>.
- Barrett, A.I., Hogan, R.J. and Forbes, R.M. (2017) Why are mixed-phase altocumulus clouds poorly predicted by large-scale models? Part 1. Physical processes. *Journal of Geophysical Research: Atmospheres*, 122(18), 9903–9926. <https://doi.org/10.1002/2016JD026321>.
- Baumgardner, D., Jonsson, H., Dawson, W., O'Connor, D. and Newton, R. (2001) The cloud, aerosol and precipitation spectrometer: a new instrument for cloud investigations. *Atmospheric Research*, 59–60, 251–264. [https://doi.org/10.1016/S0169-8095\(01\)00119-3](https://doi.org/10.1016/S0169-8095(01)00119-3).
- Bennartz, R., Shupe, M.D., Turner, D.D., Walden, V.P., Steffen, K., Cox, C.J., Kulie, M.S., Miller, N.B. and Pettersen, C. (2013) July 2012 Greenland melt extent enhanced by low-level liquid clouds. *Nature*, 496(7443), 83–86. <https://doi.org/10.1038/nature12002>.
- Bevan, S., Luckman, A., Hubbard, B., Kulesa, B., Ashmore, D., Kuipers Munneke, P., O'Leary, M., Booth, A., Sevestre, H. and McGrath, D. (2017) Centuries of intense melt on Larsen C Ice Shelf. *The Cryosphere*, 11(6), 2743–2753. <https://doi.org/10.5194/tc-2017-81>.
- Bodas-Salcedo, A., Williams, K.D., Field, P.R. and Lock, A.P. (2012) The surface downwelling solar radiation surplus over the Southern Ocean in the Met Office model: the role of midlatitude cyclone clouds. *Journal of Climate*, 25(21), 7467–7486. <https://doi.org/10.1175/JCLI-D-11-00702.1>.
- van den Broeke, M. (2005) Strong surface melting preceded collapse of Antarctic Peninsula ice shelf. *Geophysical Research Letters*, 32(12), 2–5. <https://doi.org/10.1029/2005GL023247>.
- van den Broeke, M.R., Reijmer, C., Van As, D., Van de Wal, R. and Oerlemans, J. (2005) Seasonal cycles of Antarctic surface energy balance from automatic weather stations. *Annals of Glaciology*, 41, 131–139. <https://doi.org/10.3189/172756405781813168>.
- Bromwich, D.H., Nicolas, J.P., Hines, K.M., Kay, J.E., Key, E.L., Lazara, M.A., Lubin, D., McFarquhar, G.M., Gorodetskaya, I.V., Grosvenor, D.P., Lachlan-Cope, T. and van Lipzig, N.P.M. (2012) Tropospheric clouds in Antarctica. *Reviews of Geophysics*, 50(1), 1–40. <https://doi.org/10.1029/2011RG000363>.
- Bromwich, D.H., Otieno, F.O., Hines, K.M., Manning, K.W. and Shilo, E. (2013) Comprehensive evaluation of polar weather research and forecasting model performance in the Antarctic. *Journal of Geophysical Research: Atmospheres*, 118(2), 274–292. <https://doi.org/10.1029/2012JD018139>.
- Brown, P.R.A. and Francis, P.N. (1995) Improved measurements of the ice water content in cirrus using a total-water probe. *Journal of Atmospheric and Oceanic Technology*, 12(2), 410–414. [https://doi.org/10.1175/1520-0426\(1995\)012<0410:IMOTIW>2.0.CO;2](https://doi.org/10.1175/1520-0426(1995)012<0410:IMOTIW>2.0.CO;2).
- Bush, M., Allen, T., Bain, C., Boutle, I., Edwards, J., Finnenkoetter, A., Franklin, C., Hanley, K., Lean, H., Lock, A., Manners, J., Mittermaier, M., Morcrette, C., North, R., Petch, J., Short, C., Vosper, S., Walters, D., Webster, S., Weeks, M., Wilkinson, J., Wood, N. and Zerroukat, M. (2019) The first Met Office Unified Model/JULES regional atmosphere and land configuration, RAL1. *Geoscientific Model Development Discussions*, in review, 1–48. <https://doi.org/10.5194/gmd-2019-130>.
- Cook, A.J. and Vaughan, D.G. (2010) Overview of areal changes of the ice shelves on the Antarctic Peninsula over the past 50 years. *The Cryosphere Discussions*, 3(2), 579–630. <https://doi.org/10.5194/tcd-3-579-2009>.
- Crawford, T.L. and Dobosy, R.J. (1992) A sensitive fast-response probe to measure turbulence and heat flux from any airplane. *Boundary-Layer Meteorology*, 59(3), 257–278. <https://doi.org/10.1007/BF00119816>.
- Crosier, J., Bower, K.N., Choullarton, T.W., Westbrook, C.D., Conolly, P.J., Cui, Z.Q., Crawford, I.P., Capes, G.L., Coe, H., Dorsey, J.R., Williams, P.I., Illingworth, A.J., Gallagher, M.W. and Blyth, A.M. (2011) Observations of ice multiplication in a weakly convective cell embedded in supercooled mid-level stratus. *Atmospheric Chemistry and Physics*, 11(1), 257–273. <https://doi.org/10.5194/acp-11-257-2011>.
- Edwards, J.M. and Slingo, A. (1996) Studies with a flexible new radiation code. I: Choosing a configuration for a large-scale model. *Quarterly Journal of the Royal Meteorological Society*, 122, 689–719. <https://doi.org/10.1002/qj.49712253107>.
- Elvidge, A.D., Renfrew, I.A., King, J.C., Orr, A., Lachlan-Cope, T.A., Weeks, M. and Gray, S.L. (2015) Foehn jets over the Larsen C ice shelf, Antarctica. *Quarterly Journal of the Royal Meteorological Society*, 141(688), 698–713. <https://doi.org/10.1002/qj.2382>.
- Elvidge, A.D., Renfrew, I.A., King, J.C., Orr, A. and Lachlan-Cope, T.A. (2016) Foehn warming distributions in nonlinear and linear flow regimes: a focus on the Antarctic Peninsula. *Quarterly Journal of the Royal Meteorological Society*, 142(695), 618–631. <https://doi.org/10.1002/qj.2489>.
- Field, P.R., Cotton, R.J., McBeath, K., Lock, A.P., Webster, S. and Allan, R.P. (2014) Improving a convection-permitting model simulation of a cold air outbreak. *Quarterly Journal of the Royal Meteorological Society*, 140, 124–138. <https://doi.org/10.1002/qj.2116>.
- Furtado, K. and Field, P. (2017) The role of ice microphysics parametrizations in determining the prevalence of supercooled liquid water in high-resolution simulations of a Southern Ocean midlatitude cyclone. *Journal of the Atmospheric Sciences*, 74, 2001–2021. <https://doi.org/10.1175/JAS-D-16-0165.1>.
- Furtado, K., Field, P.R., Boutle, I.A., Morcrette, C.J. and Wilkinson, J.M. (2016) A physically based subgrid parameterization for the production and maintenance of mixed-phase clouds in a general circulation model. *Journal of the Atmospheric Sciences*, 73(1), 279–291. <https://doi.org/10.1175/JAS-D-15-0021.1>.
- Grosvenor, D.P., Choullarton, T.W., Lachlan-Cope, T., Gallagher, M.W., Crosier, J., Bower, K.N., Ladkin, R.S. and Dorsey, J.R. (2012) *In-situ* aircraft observations of ice concentrations within clouds over the Antarctic Peninsula and Larsen Ice Shelf. *Atmospheric Chemistry and Physics*, 12(23), 11275–11294. <https://doi.org/10.5194/acp-12-11275-2012>.
- Grosvenor, D.P., Field, P.R., Hill, A.A. and Shipway, B.J. (2017) The relative importance of macrophysical and cloud albedo changes for aerosol-induced radiative effects in closed-cell stratocumulus: insight from the modelling of a case study. *Atmospheric Chemistry and Physics*, 17(8), 5155–5183. <https://doi.org/10.5194/acp-17-5155-2017>.
- Hines, K.M., Bromwich, D.H., Wang, S.H., Silber, I., Verlinde, J. and Lubin, D. (2019) Microphysics of summer clouds in central

- West Antarctica simulated by the Polar Weather Research and Forecasting model (WRF) and the Antarctic Mesoscale Prediction System (AMPS). *Atmospheric Chemistry and Physics*, 19(19), 12431–12454. <https://doi.org/10.5194/acp-19-12431-2019>.
- Hyder, P., Edwards, J.M., Allan, R.P., Hewitt, H.T., Bracegirdle, T.J., Gregory, J.M., Wood, R.A., Meijers, A.J.S., Mulcahy, J., Field, P.R., Furtado, K., Bodas-Salcedo, A., Williams, K.D., Copsey, D., Josey, S.A., Liu, C., Roberts, C.D., Sanchez, C., Ridley, J., Thorpe, L., Hardiman, S.C., Mayer, M., Berry, D.I. and Belcher, S.E. (2018) Critical Southern Ocean climate model biases traced to atmospheric model cloud errors. *Nature Communications*, 9(1), 3625. <https://doi.org/10.1038/s41467-018-05634-2>.
- Kalesse, H., de Boer, G., Solomon, A., Oue, M., Ahlgrimm, M., Zhang, D., Shupe, M.D., Luke, E. and Protat, A. (2016) Understanding rapid changes in phase partitioning between cloud liquid and ice in stratiform mixed-phase clouds: an Arctic case study. *Monthly Weather Review*, 144(12), 4805–4826. <https://doi.org/10.1175/MWR-D-16-0155.1>.
- Kay, J.E., L'Ecuyer, T., Gettelman, A., Stephens, G., and O'Dell, C. (2008) The contribution of cloud and radiation anomalies to the 2007 Arctic sea ice extent minimum. *Geophysical Research Letters*, 35(8), 1–5. <https://doi.org/10.1029/2008GL033451>.
- King, J.C., Lachlan-Cope, T.A., Ladkin, R.S. and Weiss, A. (2008) Airborne measurements in the stable boundary layer over the Larsen Ice Shelf, Antarctica. *Boundary-Layer Meteorology*, 127(3), 413–428. <https://doi.org/10.1007/s10546-008-9271-4>.
- King, J.C., Gadian, A., Kirchgassner, A., Kuipers Munneke, P., Lachlan-Cope, T.A., Orr, A., Reijmer, C., van den Broeke, M.R., Van Wessem, J.M. and Weeks, M. (2015) Validation of the summertime surface energy budget of Larsen C Ice Shelf (Antarctica) as represented in three high-resolution atmospheric models. *Journal of Geophysical Research: Atmospheres*, 120(4), 1335–1347. <https://doi.org/10.1002/2014JD022604>.
- Klein, S.A., McCoy, R.B., Morrison, H., Ackerman, A.S., De Boer, G., Chen, M., Cole, J.N.S., Genio, D.D., Foster, M.J., Fridlind, A., Golaz, J.-C., Hashino, T., Jerry, Y., Hoose, C., Khairoutdinov, M.F., Larson, V.E., Liu, X., McFarquhar, G.M., Menon, S., Neggers, R.A.J., Park, S., Michael, R., Schmidt, J.M., Sednev, I., Shipway, B.J., Shupe, M.D., Spangenberg, D.A., Sud, Y.C., Turner, D.D., Veron, D.E., Von, K., Walker, G.K., Wang, Z., Wolf, A.B. and Xie, S. (2009) Intercomparison of model simulations of mixed-phase clouds observed during the ARM Mixed-Phase Arctic Cloud Experiment. I: Single-layer cloud. *Quarterly Journal of the Royal Meteorological Society*, 135, 979–1002. <https://doi.org/10.1002/qj.416>.
- Kuipers Munneke, P., van den Broeke, M.R., Reijmer, C.H., Helsen, M.M., Boot, W., Schneebeli, M. and Steffen, K. (2009) The role of radiation penetration in the energy budget of the snowpack at Summit, Greenland. *The Cryosphere*, 3(1), 155–165. <https://doi.org/10.5194/tcd-3-277-2009>.
- Kuipers Munneke, P., van den Broeke, M.R., King, J.C., Gray, T. and Reijmer, C.H. (2012) Near-surface climate and surface energy budget of Larsen C ice shelf, Antarctic Peninsula. *The Cryosphere*, 6(2), 353–363. <https://doi.org/10.5194/tc-6-353-2012>.
- Lachlan-Cope, T. (2010) Antarctic clouds. *Polar Research*, 29(2), 150–158. <https://doi.org/10.1111/j.1751-8369.2010.00148.x>.
- Lachlan-Cope, T., Listowski, C. and O'Shea, S. (2016) The microphysics of clouds over the Antarctic Peninsula – Part 1: Observations. *Atmospheric Chemistry and Physics*, 16, 15605–15617. <https://doi.org/10.5194/acp-16-15605-2016>.
- Lenaerts, J.T.M., Van Tricht, K., Lhermitte, S. and L'Ecuyer, T.S. (2017) Polar clouds and radiation in satellite observations, reanalyses, and climate models. *Geophysical Research Letters*, 44(7), 3355–3364. <https://doi.org/10.1002/2016GL072242>.
- Lenaerts, J.T.M., Ligtenberg, S.R.M., Medley, B., Van de Berg, W.J., Konrad, H., Nicolas, J.P., Van Wessem, J.M., Trusel, L.D., Mulvaney, R., Tuckwell, R.J., Hogg, A.E. and Thomas, E.R. (2018) Climate and surface mass balance of coastal West Antarctica resolved by regional climate modelling. *Annals of Glaciology*, 59(76, part 1), 29–41. <https://doi.org/10.1017/aog.2017.42>.
- Listowski, C. and Lachlan-Cope, T. (2017) The microphysics of clouds over the Antarctic Peninsula – Part 2: Modelling aspects within Polar WRF. *Atmospheric Chemistry and Physics*, 17, 10195–10221. <https://doi.org/10.5194/acp-17-10195-2017>.
- Listowski, C., Delanoë, J., Kirchgassner, A., Lachlan-Cope, T. and King, J. (2019) Antarctic clouds, supercooled liquid water and mixed phase investigated with DARDAR: geographical and seasonal variations. *Atmospheric Chemistry and Physics*, 19(10), 6771–6808. <https://doi.org/10.5194/acp-19-6771-2019>.
- Lock, A. (2011) Stable boundary layer modelling at the Met Office. In: *ECMWF GABLS Workshop on Diurnal cycles and the stable boundary layer*, 7–10 November 2011, 137–148.
- Miller, N.B., Shupe, M.D., Cox, C.J., Walden, V.P., Turner, D.D. and Steffen, K. (2015) Cloud radiative forcing at Summit, Greenland. *Journal of Climate*, 28(15), 6267–6280. <https://doi.org/10.1175/JCLI-D-15-0076.1>.
- Nicolas, J.P., Vogelmann, A.M., Scott, R.C., Wilson, A.B., Cadeddu, M.P., Bromwich, D.H., Verlinde, J., Lubin, D., Russell, L.M., Jenkinson, C., Powers, H.H., Ryzek, M., Stone, G. and Wille, J.D. (2017) January 2016 extensive summer melt in West Antarctica favoured by strong El Niño. *Nature Communications*, 8(May), 1–10. <https://doi.org/10.1038/ncomms15799>.
- Orr, A., Phillips, T., Webster, S., Elvidge, A., Weeks, M., Hosking, S. and Turner, J. (2014) Met Office Unified Model high-resolution simulations of a strong wind event in Antarctica. *Quarterly Journal of the Royal Meteorological Society*, 140(684), 2287–2297. <https://doi.org/10.1002/qj.2296>.
- Scambos, T.A., Hulbe, C., Fahnestock, M. and Bohlander, J. (2000) The link between climate warming and break-up of ice shelves in the Antarctic Peninsula. *Journal of Glaciology*, 46(154), 516–530. <https://doi.org/10.3189/172756500781833043>.
- Scambos, T., Hulbe, C. and Fahnestock, M. (2003) Climate-induced ice shelf disintegration in the Antarctic Peninsula. In: Domack, E., Levente, A., Burnet, A., Bindschadler, R., Convey, P. and Kirby, M. (Eds.) *Antarctic Peninsula Climate Variability: Historical and Paleoenvironmental Perspectives*, Antarctic Research Series, Washington, DC: American Geophysical Union, Vol. 79, pp. 79–92. <https://doi.org/doi:10.1029/AR079p0079>.
- Smith, R.N.B. (1990) A scheme for predicting layer clouds and their water content in a general circulation model. *Quarterly Journal of the Royal Meteorological Society*, 116, 435–460. <https://doi.org/10.1002/qj.49711649210>.
- Souvereinjs, N., Gossart, A., Demuzere, M., Lenaerts, J.T.M., Medley, B., Gorodetskaya, I.V., Vanden Broucke, S. and van Lipzig, N.P.M. (2019) A new regional climate model for POLAR-CORDEX: evaluation of a 30-year hindcast with COSMO-CLM 2 over

- Antarctica. *Journal of Geophysical Research: Atmospheres*, 124(3), 1405–1427. <https://doi.org/10.1029/2018JD028862>.
- Tan, I. and Storelvmo, T. (2016) Sensitivity study on the influence of cloud microphysical parameters on mixed-phase cloud thermodynamic phase partitioning in CAM5. *Journal of the Atmospheric Sciences*, 73(2), 709–728. <https://doi.org/10.1175/JAS-D-15-0152.1>.
- Turner, J., Colwell, S.R., Marshall, G.J., Lachlan-Cope, T.A., Carleton, A.M., Jones, P.D., Lagun, V., Reid, P.A. and Iagovkina, S. (2005) Antarctic climate change during the last 50 years. *International Journal of Climatology*, 25(3), 279–294. <https://doi.org/10.1002/joc.1130>.
- Turner, J., Lu, H., White, I., King, J.C., Phillips, T., Hosking, J.S., Bracegirdle, T.J., Marshall, G.J., Mulvaney, R. and Deb, P. (2016) Absence of 21st century warming on Antarctic Peninsula consistent with natural variability. *Nature*, 535(7612), 411–415. <https://doi.org/10.1038/nature18645>.
- Van Wessem, J.M., Reijmer, C.H., Lenaerts, J.T.M., Van de Berg, W.J., van den Broeke, M.R. and Van Meijgaard, E. (2014) Updated cloud physics in a regional atmospheric climate model improves the modelled surface energy balance of Antarctica. *The Cryosphere*, 8(1), 125–135. <https://doi.org/10.5194/tc-8-125-2014>.
- Van Wessem, J.M., van de Berg, W.J., Noël, B.P., van Meijgaard, E., Birnbaum, G., Jakobs, C.L., Krüger, K., Lenaerts, J.T.M., Lhermitte, S., Ligtenberg, S.R.M., Medley, B., Reijmer, C.H., van Tricht, K., Trusel, L.D., van Ulft, L.H., Wouters, B., Wuite, J. and van den Broeke, M.R. (2018) Modelling the climate and surface mass balance of polar ice sheets using RACMO2. Part 2: Antarctica (1979–2016). *The Cryosphere*, 12(4), 1479–1498. <https://doi.org/10.5194/tc-2017-202>.
- Vergara-Temprado, J., Miltenberger, A.K., Furtado, K., Grosvenor, D.P., Shipway, B.J., Hill, A.A., Wilkinson, J.M., Field, P.R., Murray, B.J. and Carslaw, K.S. (2018) Strong control of Southern Ocean cloud reflectivity by ice-nucleating particles. *Proceedings of the National Academy of Sciences*, 115(11), 2687–2692. <https://doi.org/10.1073/pnas.1721627115>.
- Walters, D., Boutle, I., Brooks, M., Melvin, T., Stratton, R., Vosper, S., Wells, H., Williams, K., Wood, N., Allen, T., Bushell, A., Copsey, D., Earnshaw, P., Edwards, J., Gross, M., Hardiman, S., Harris, C., Heming, J., Klingaman, N., Levine, R., Manners, J., Martin, G., Milton, S., Mittermaier, M., Morcrette, C., Riddick, T., Roberts, M., Sanchez, C., Selwood, P., Stirling, A., Smith, C., Suri, D., Tennant, W., Luigi Vidale, P., Wilkinson, J., Willett, M., Woolnough, S. and Xavier, P. (2017) The Met Office Unified Model Global Atmosphere 6.0/6.1 and JULES Global Land 6.0/6.1 configurations. *Geoscientific Model Development*, 10(4), 1487–1520. <https://doi.org/10.5194/gmd-10-1487-2017>.
- Wilson, D.R. and Ballard, S.P. (1999) A microphysically based precipitation scheme for the UK Meteorological Office Unified Model. *Quarterly Journal of the Royal Meteorological Society*, 125(557), 1607–1636. <https://doi.org/10.1002/qj.49712555707>.
- Wilson, D.R., Bushell, A.C., Kerr-Munslow, A.M., Price, J.D. and Morcrette, C.J. (2008) PC2: a prognostic cloud fraction and condensation scheme. I: Scheme description. *Quarterly Journal of the Royal Meteorological Society*, 134(637), 2093–2107. <https://doi.org/10.1002/qj.333>.
- Zhang, T., Stamnes, K. and Bowling, S.A. (1996) Impact of clouds on surface radiative fluxes and snowmelt in the Arctic and subarctic. *Journal of Climate*, 9(9), 2110–2123. [https://doi.org/10.1175/1520-0442\(1996\)009<2110:IOCOSR>2.0.CO;2](https://doi.org/10.1175/1520-0442(1996)009<2110:IOCOSR>2.0.CO;2).

How to cite this article: Gilbert E, Orr A, King JC, *et al.* Summertime cloud phase strongly influences surface melting on the Larsen C ice shelf, Antarctica. *Q J R Meteorol Soc.* 2020;146:1575–1589. <https://doi.org/10.1002/qj.3753>

APPENDIX A: AIRCRAFT INSTRUMENTATION AND DATA TREATMENT

Cloud microphysics are observed using the British Antarctic Survey's instrumented De Havilland Twin Otter aircraft, which measures standard meteorological variables: total temperature is measured with Rosemount probes, static pressure is measured using in-built aircraft sensors, humidity is observed by a Vaisala humicap sensor and cooled mirror hygrometer, and three-dimensional winds are measured using a Best Aircraft Turbulence (BAT) probe (Crawford and Dobosy, 1992), mounted on a boom fitted to the nose of the aircraft. Upwelling and downwelling radiative fluxes (short-wave and long-wave) are measured using Eppley pyranometers and pyrgeometers mounted to the belly and roof of the aircraft, respectively. Surface temperatures are measured using a downward-looking infrared thermometer (Heitronics KT19.82). A full description of the aircraft's instrumentation can be found in King *et al.* (2008). The aircraft can be adapted to measure specific areas of interest, and during the OFCAP campaign was fitted with a Droplet Measurement Technologies Cloud, Aerosol and Precipitation Spectrometer (CAPS probe: Baumgardner *et al.*, 2001) to sample cloud properties. The probe contains three separate instruments: a Cloud and Aerosol Spectrometer (CAS) which measures the diameter of small cloud particles 0.5–50 µm, a Cloud Imaging Probe (CIP) which images larger cloud and precipitation-sized particles of 25 µm – 1.5 mm diameter using a charge-coupled device array, and a hotwire liquid water contents (LWC) sensor, which is used to validate CAS data.

In-cloud particles observed by the CAS instrument are all assumed to be liquid droplets, whereas those observed by the CIP must be post-processed to determine their phase. After data are quality controlled and processed using the method of Crosier *et al.* (2011), cloud particles are segregated into ice and liquid using the technique of Lachlan-Cope *et al.* (2016) by determining their circularity, C , defined as:

$$C = P^2 / 4 \pi A, \quad (\text{A1})$$

where P is the particle perimeter as measured by the instrument and A is the particle area, which must be a minimum of 50 pixels (or $\sim 200 \mu\text{m}$) to be detected. Particles with $0.9 \leq C \leq 1.2$ are considered to be circular and are thus classified as drops, while those with $C \geq 1.4$ are classified as ice. Following visual inspection of the data from the flights considered, particles with intermediate circularity $1.2 \leq C \leq 1.4$ are classified as ice, as in Lachlan-Cope *et al.* (2016). Ice water contents are then calculated with the mass-dimensional relationship of Brown and Francis (1995).

Only in-cloud data are used to compute mean profiles, where cloud is defined as in Lachlan-Cope *et al.* (2016) when the CAS instrument measures either number concentrations above 1 cm^{-3} of droplet-sized particles greater than $1 \mu\text{m}$ in diameter or when the CIP instrument measures number concentrations of ice particles above $1.0 \times 10^{-8} \text{ cm}^{-3}$.

APPENDIX B: AUTOMATIC WEATHER STATION (AWS) DATA

Observations of surface energy fluxes and meteorology are retrieved from the Larsen North automatic weather station (AWS14), which is set up as described in Kuipers Munneke *et al.* (2009). Observations of air temperature, pressure, relative humidity, wind speed and direction, and radiative fluxes (up- and downwelling components of long-wave and short-wave) are made directly, while the sensible and latent heat fluxes are calculated using the bulk aerodynamic method. An energy balance model (van den Broeke *et al.*, 2005) is applied to compute the energy balance of the snowpack after the raw data have been corrected using the method of Kuipers Munneke *et al.* (2012).

APPENDIX C: NUMERICAL WEATHER PREDICTION MODEL DESCRIPTION AND PARAMETRIZATION SCHEMES

The Met Office Unified Model (MetUM) is a numerical weather prediction model used for operational and research purposes. Its dynamical core is non-hydrostatic and uses semi-implicit time-stepping and semi-Lagrangian advection (Walters *et al.*, 2017). Model equations are solved on a staggered Arakawa-C grid in the horizontal and with Charney–Phillips staggering in the vertical, with a hybrid height vertical coordinate that is terrain-following near the surface. It is run in atmosphere-only mode and configured similarly to Orr *et al.* (2014), although in contrast to that work, this study uses just one nested domain at 1.5 km horizontal grid

spacing with a 60 second time step. This inner nest takes input from a global model that has $\sim 17 \text{ km}$ resolution in the midlatitudes, which is forced at the boundaries with Met Office global operational analyses.

Simulations are run in forecast mode as described in the main text: re-initialisations occur at 0000 UTC and 1200 UTC, with only the $t + 12$ to $t + 24$ part of the forecast retained. The case-study is initialised 12 hours prior to the flight, while the OFCAP simulation comprises a series of forecasts concatenated together. All quantities of interest are outputted as instantaneous values every 15 min, except meteorological variables, which are outputted hourly. During the OFCAP period, all variables are outputted as hourly instantaneous values.

The radiation scheme (SOCRATES) is based on Edwards and Slingo (1996), which calculates surface radiative fluxes prognostically using six short-wave and nine long-wave absorption bands. Absorption and scattering by cloud particles are treated by applying “thick averaging” to calculate droplet effective radius from number concentrations computed by the microphysics, and ice crystals are parametrized according to Baran *et al.* (2014).

The operational single-moment microphysics scheme used in all experiments is based on Wilson and Ballard (1999) and represents condensate mass mixing ratios only, with prescribed number concentrations over land (including ice shelves) and open water. The scheme is three-phase, representing cloud liquid water, rain and snow (which encompasses all ice in the grid box) prognostically. Microphysical processes produce or deplete condensate in each layer as follows: liquid droplets are formed via condensation, and are removed by droplet settling, autoconversion to rain drops, freezing during the ice nucleation process and riming. Rain droplets form from cloud water via autoconversion, from cloud water or other rain droplets via sedimentation or accretion, and from ice by melting. Rain is depleted by sedimentation or evaporation, or converted into ice during homogeneous ice nucleation or ice crystal capture. Ice is produced directly from the vapour phase via vapour diffusion (the Wegener–Bergeron–Findeisen process), or from the liquid phase via rain droplet capture or riming, and is lost due to sedimentation, sublimation and melting. Heterogeneous ice nucleation occurs when the temperature is below a specified threshold and liquid water is present in a grid box, representing an immersion freezing or condensation mechanism. All experiments use a modified threshold of $-18 \text{ }^\circ\text{C}$ rather than the default $-10 \text{ }^\circ\text{C}$, as this modification was shown by Field *et al.* (2014) to improve the representation of mixed-phase cloud because it forces supercooled liquid to remain liquid at colder temperatures.